Results in Physics 8 (2018) 206–212

Contents lists available at ScienceDirect

Results in Physics

journal homepage: www.journals.elsevier.com/results-in-physics

Numerical simulation for aspects of homogeneous and heterogeneous reactions in forced convection flow of nanofluid

Tasawar Hayat [a,b], Faisal Shah [a], Muhammad Ijaz Khan [a,*], Ahmed Alsaedi [b]

[a] Department of Mathematics, Quaid-I-Azam University, 45320 Islamabad 44000, Pakistan
[b] Nonlinear Analysis and Applied Mathematics (NAAM) Research Group, Department of Mathematics, Faculty of Science, King Abdulaziz University, Jeddah 21589, Saudi Arabia

ARTICLE INFO

Article history:
Received 17 May 2017
Received in revised form 26 October 2017
Accepted 30 November 2017
Available online 6 December 2017

Keywords:
Mixed convection
Stagnation point flow
Homogeneous-heterogeneous reactions
Nanofluids

ABSTRACT

Mixed convection stagnation point flow of nanofluid by a vertical permeable circular cylinder has been addressed. Water is treated as ordinary liquid while nanoparticles include aluminium oxide, copper and titanium dioxide. Homogeneous-heterogeneous reactions are considered. The nonlinear higher order expressions are changed into first ordinary differential equations and then solved by built-in-Shooting method in mathematica. The results of velocity, temperature, concentration, skin friction and local Nusselt number are discussed. Our results demonstrate that surface drag force and heat transfer rate are enhanced linearly for higher estimation of curvature parameter. Further surface drag force decays for aluminium oxide and it enhances for copper nanoparticle. Heat transfer rate enhances with increasing all three types of nanoparticles. In addition, the lowest heat transfer rate is obtained in case of titanium dioxide when compared with copper and aluminium oxide.

Introduction

Many industrial liquids have low thermal conductivity which limits the quality of final product during engineering procedure. Pioneer concept of nanomaterial with improved thermal conductivity was given by Choi [1]. Nanotechnology has significance in atomic reactors, chemical process, energy process, mechanical cooling, indicative tests, extraction of geothermal force, disease treatment, heat exchangers and some applications in micro scale fluidic. Convective transport in nanoliquids subject to thermophoresis and Brownian effects is explored by Boungiorno [2]. Effect of nanomaterials on natural convective flow past a vertical surface is examined by Kuznetsov and Nield [3]. Later on the same problem is discussed by Nield and Kuznetsov [4] for a porous space. MHD natural convection carbon nanotubes flow has been studied by Ellahi et al. [5]. Nanofluid flow of forced convection with magnetic field utilizing LBM is explored by Sheikholeslami et al. [6]. Convective heat transfer characteristics of Al_2O_3 nanomaterials submerged in water is studied by Hwang et al. [7]. Kumaresan et al. [8] discuused convective heat transfer characteristics of secondary refrigerant based nanoliquids. Flow of nanoliquid in a porous channel is addressed by Hatami et al. [9]. Farooq et al. [10] analyzed MHD stagnation point flow of Jeffrey nanomaterial in the presence of radiation. Mabood et al. [11] addressed mixed convection unsteady flow of nanofluid with viscous dissipation. Convective flow of Cu-water nanomaterial by a rotating cone using is studied by Dinarvand and Pop [12]. Few more recent studies about flows of nanofluids can be visualized through the attempts [13–18].

Heat transfer in flow over a stretchable surface has widespread applications. Due to tremendous applications in engineering and sciences, a large amount of work is focussed at present in this area, drawing of plastic sheets, fibres glass, paper production, metal spinning, fibre and wire coating, food stuff processing, continuous casting, exchangers and chemical processing equipment. All procedures of coating involve a smooth glossy surface to fulfill the necessities for appearance, transparency, strength and low fraction. Crane [19] initiated flow of viscous liquid by a stretched surface. MHD stagnation point flow of rate type nanofluid with thermophoresis is investigated by Bai et al. [20]. Heat transfer in flow of micropolar liquid over a porous stretching surface is examined by Turkyilmazoglu [21]. Melting heat transfer and homogeneous heterogeneous reactions in MHD viscous liquid flow by a stretchable surface is explored by Hayat et al. [22]. Magnetohydrodynamic nanofluid flow past a porous plate with radiation, chemical reaction and rotation is considered by Reddya et al. [23]. Consequences of convective boundary conditions and chemical reaction on flow due to a plate are considered by Rout et al. [24]. Application of non-Fourier heat flux in flow of Jeffrey liquid with temperature dependent thermal conductivity is studied by Hayat

* Corresponding author.
E-mail address: mikhan@math.qau.edu.pk (M.I. Khan).

https://doi.org/10.1016/j.rinp.2017.11.035
2211-3797/

et al. [25]. Hayat et al. [26] also investigated chemically reactive flow and non-Fourier heat flux in flow by a stretching surface. Viscous dissipation in three dimensional flow of viscous nanoliquid is reported by Mahanthesh et al. [27]. Numerical simulation is performed in this work. Hayat et al. [28] examined flow of Burgers nanoliquid in presence of magnetohydrodynamics (MHD) and convective condition. Li et al. [29] discussed characteristics of non-Fourier heat conduction in MHD nanofluid flow by a stretched surface. Stretched flow of Oldroyd-B fluid with Cattaneo-Chrsitov heat flux is inspected by Hayat et al. [30].

Prime objective of this analysis is to analyze the impacts of thermal radiation and mixed convection in stagnation point flow of viscous nanofluid by a vertical permeable cylinder. Homogeneous-heterogeneous reactions are also accounted. Induced electric and magnetic fields are absent. Computations for strong nonlinear systems are presented after non-dimensionalization through built-in-Shooting method [31–35]. Graphical analysis for various influential variables is addressed in detail.

Formulation

We investigate the mixed convection stagnation point flow of an electrically conducting incompressible viscous nanofluid by a vertical permeable circular cylinder of radius a. We choose cylindrical coordinate system such that x is along the stretching cylinder and r normal to x. Here u and w are the velocity components in x and r directions (see Fig. 1). A magnetic field of strength B_0 is exerted along radial direction. We represent T_w as temperature of cylinder and T_∞ the ambient temperature. For the formation of compound $3B$ the fluid phase reaction is [22,26]:

$$A + 2B \rightarrow 3B, \quad rate = k_c a^* b^{*2},$$

$$A + B \rightarrow 3B, \quad rate = k_s a^* b^{*2}.$$

In above expressions A and B denote chemical species, a^* and b^* the concentrations and k_c and k_s the rate constants. Both reaction processes are isothermal. The subjected problems statements are

$$\frac{\partial(ru)}{\partial x} + \frac{\partial(rw)}{\partial r} = 0, \tag{1}$$

$$u\frac{\partial u}{\partial x} + w\frac{\partial u}{\partial r} = u_e\frac{du_e}{dx} + \nu_{nf}\left(\frac{\partial^2 u}{\partial r^2} + \frac{1}{r}\frac{\partial u}{\partial r}\right) + \frac{\sigma_{nf}B_0^2}{\rho_{nf}}(u_e - u) + \frac{\phi\rho_s\beta_s + (1-\phi)\rho_f\beta_f}{\rho_{nf}}g(T - T_\infty), \tag{2}$$

$$u\frac{\partial T}{\partial x} + w\frac{\partial T}{\partial r} = \alpha_{nf}\left(\frac{\partial^2 T}{\partial y^2} + \frac{1}{r}\frac{\partial T}{\partial r}\right), \tag{3}$$

$$u\frac{\partial a^*}{\partial x} + w\frac{\partial a^*}{\partial r} = D_A\left(\frac{\partial^2 a^*}{\partial r^2} + \frac{1}{r}\frac{\partial a^*}{\partial r}\right) - k_c a^* b^{*2}, \tag{4}$$

$$u\frac{\partial b^*}{\partial x} + w\frac{\partial b^*}{\partial r} = D_B\left(\frac{\partial^2 b^*}{\partial r^2} + \frac{1}{r}\frac{\partial b^*}{\partial r}\right) + k_c a^* b^{*2}. \tag{5}$$

with

$$u = u_w(x) = u_0\left(\frac{x}{l}\right), \quad w = V_w^*, \quad T = T_w(x) = T_\infty + \Delta T\left(\frac{x}{l}\right),$$
$$D_A\frac{\partial a^*}{\partial r} = k_s a^*, \quad D_B\frac{\partial b^*}{\partial r} = -k_s a^* \text{ at } r = a,$$
$$u \rightarrow u_e(x) = u_\infty\left(\frac{x}{l}\right), \quad T \rightarrow T_\infty, \quad a^* \rightarrow a_o, \quad b^* \rightarrow 0 \text{ when } r \rightarrow \infty. \tag{6}$$

In above equations u and w indicate the velocity components, u_e the free stream velocity, where $V_w^* < 0$ corresponds to suction and $V_w^* > 0$ for injection, u_w the stretching velocity, ν_{nf} the kinematic viscosity, T the temperature, T_∞ the ambient temperature, ρ_f the density of nanofluid, g the gravity acceleration, ϕ the nanoparticle volume friction, β the thermal expansion coefficient, a^* and b^* the concentrations, l the characteristics length, B_0 the uniform magnetic field, σ the electrical conductivity, D_A and D_B the diffusion species, a_0 the positive dimensional constant, k_s the heat transfer coefficient, β the coefficient of thermal expansion and α_{nf} thermal diffusivity. Their definitions are

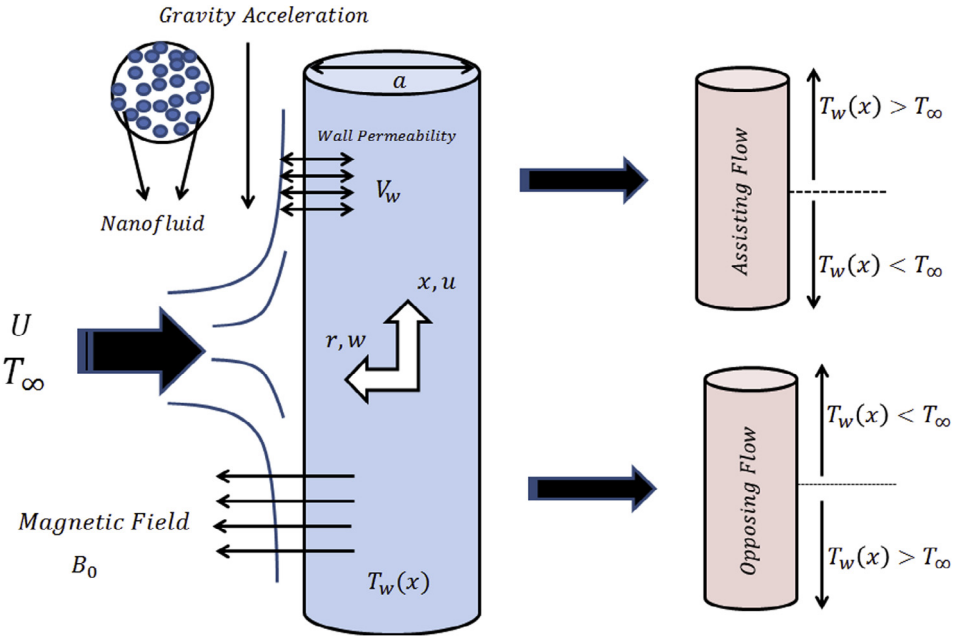

Fig. 1. Flow configuration.

$$\nu_{nf} = \frac{\mu_f}{(1-\phi)^{2.5}[(1-\phi)\rho_f + \phi\rho_s]}, \tag{7}$$

$$\rho_{nf} = (1-\phi)\rho_f + \phi\rho_s, \tag{8}$$

$$\alpha_{nf} = \frac{k_{nf}}{(\rho C_p)_{nf}}, \tag{9}$$

$$(\rho C_p)_{nf} = (1-\phi)(\rho C_p)_f + \phi(\rho C_p)_s, \tag{10}$$

$$\frac{k_{nf}}{k_f} = \frac{(k_s+2k_f) - 2\phi(k_f-k_s)}{(k_s+2k_f) + \phi(k_f-k_s)}, \tag{11}$$

in which ϕ nanoparticle volume fraction, ρ_f and ρ_s density of fluid and solid particles, μ_f dynamic viscosity of fluid and k_f and k_{nf} thermal conductivities of fluid and nanomaterial respectively. Table 1

Having transformations

$$\eta = \frac{r^2-a^2}{2lv_f}\left(\frac{U_\infty l v_f}{a^2}\right)^{\frac{1}{2}},\ \psi = \left(\frac{U_\infty v_f a^2}{l}\right)^{\frac{1}{2}} x f(\eta),\ u = \left(\frac{1}{r}\right)\left(\frac{\partial\psi}{\partial r}\right),$$
$$w = -\left(\frac{1}{r}\right)\left(\frac{\partial\psi}{\partial x}\right),\ T - T_\infty = \triangle T\left(\frac{x}{l}\right)\theta(\eta),\ g(\eta) = \frac{a^*}{a_o},\ h(\eta) = \frac{b^*}{b_o}, \tag{12}$$

the incompressibility constraint is verified trivially while expressions (2)–(6) are reduced to

$$\left.\begin{aligned}&\frac{1}{(1-\phi)^{2.5}\left(1-\phi+\phi\frac{\rho_s}{\rho_f}\right)}[(1+2\gamma\eta)f''' + 2\gamma f''] + f'^2 + \beta^{*2}\\ &+\frac{M}{\left(1-\phi+\phi\frac{\rho_s}{\rho_f}\right)}[\beta^* - f'] + \frac{\left(1-\phi+\phi\frac{\rho_s\beta_s}{\rho_f\beta_f}\right)}{\left(1-\phi+\phi\frac{\rho_s}{\rho_f}\right)}\lambda\theta = 0,\end{aligned}\right\} \tag{13}$$

$$\frac{\frac{k_{nf}}{k_f}}{\left(1-\phi+\phi\frac{(\rho c_p)_s}{(\rho c_p)_f}\right)}[(1+2\gamma\eta)\theta'' + 2\gamma\theta'] + \Pr(f\theta' + f'\theta) = 0, \tag{14}$$

$$\frac{1}{Sc}[(1+2\gamma\eta)g'' + 2\gamma g'] + fg' - kgh^2 = 0, \tag{15}$$

$$\frac{\delta}{Sc}[(1+2\gamma\eta)h'' + 2\gamma h'] + fh' - kgh^2 = 0, \tag{16}$$

$$f = V_w,\quad f' = 0,\quad \theta = 1,\quad g' = k_s g,\quad \delta h' = -k_s g \text{ at } \eta = 0,$$
$$f' \to \beta^*,\quad \theta \to 0,\quad g \to 0,\quad h \to 0 \text{ when } \eta \to \infty. \tag{17}$$

Here $\lambda\left(=\frac{Gr}{\mathrm{Re}^2}\right)$ denotes the mixed convection parameter, $Gr\left(=\frac{g\beta_f\Delta Tl^3}{\nu_f^2}\right)$ the Grashof number, $\gamma\left(=\frac{\gamma_f l}{U_\infty a^2}\right)^{0.5}$ the curvature parameter, $V_w\left(=\frac{r}{a}\left(\frac{l}{\nu_f U_\infty}\right)^{0.5} V_w^*\right)$ permeability parameter, $M\left(=\frac{\sigma B_0^2}{\rho_f\left(\frac{U_\infty}{l}\right)}\right)$ the magnetic parameter, $K\left(=\frac{k_c a_o^2 l}{U_\infty}\right)$ the homogeneous parameter, $\beta^*\left(=\frac{u_\infty}{u_0}\right)$ the velocities ratio, $K_s\left(\frac{k_s}{D_A}\sqrt{\frac{\nu_f l}{U_\infty}}\right)$ the heterogeneous parameter, $\mathrm{Re}_x\left(=\frac{U_\infty l}{\nu_f^2}\right)$ the local Reynolds number, $\Pr\left(=\frac{\nu}{\alpha}\right)$ the Prandtl number and $\delta\left(=\frac{D_B}{D_A}\right)$ the diffusion coefficient with ratio of mass.

Putting $\delta = 1$ and $g(\eta) + h(\eta) = 1$ then Eqs. (10)–(12) become

$$\frac{1}{Sc}[(1+2\gamma\eta)g'' + 2\gamma g'] + fg' - Kg(1-g)^2 = 0, \tag{18}$$

$$g' = K_s g \text{ at } \eta \to 0,\quad g \to 1 \text{ at } \eta \to \infty. \tag{19}$$

Mathematical expression for surface drag force and heat transfer rate are

$$C_f = \frac{\tau_w}{\rho_f U_\infty^2},\quad Nu_x = \frac{lq_w}{k_f\triangle T}, \tag{20}$$

where

$$\tau_w = \mu_{nf}\Big|_{r=a}\frac{\partial u}{\partial r}\Big|_{r=a},$$
$$q_w = -k_f\left(\frac{\partial T}{\partial r}\right)_{r=a}. \tag{21}$$

Invoking Eq. (21) in Eq. (20) we take the following dimensionless forms

$$\mathrm{Re}_x^{0.5} C_{fx} = \left(\frac{\bar{x}}{(1-\phi)^{2.5}} f''(0)\right),\quad \mathrm{Re}_x^{-0.5} Nu_x = -\frac{k_{nf}}{k_f}\bar{x}\theta'(0), \tag{22}$$

in which $\bar{x} = \frac{x}{l}$.

Discussion

The differential systems consisting of Eqs. (13), (14), (18) and (17), (19) have been solved numerically by built-in-Shooting method in mathematica. Numerical computations are carried out for several set of variables known as Prandtl number (Pr), mixed convection parameter (λ), curvature parameter (γ), permeability parameter (V_w), magnetic parameter (M), Schmidt number (Sc), nanoparticle volume fraction (ϕ), homogeneous reaction parameter (k) and heterogeneous reaction parameter (k_s). For physical insights of velocity $f'(\eta)$, temperature $\theta(\eta)$ and concentration $g(\eta)$, the Figs. 2–17 have been displayed.

Influence of curvature (γ) parameter on the fluid velocity field for positive values of mixed convection (λ) parameter is shown in Fig. 2. There is an enhancement of $f'(\eta)$ for larger (γ). Since for lager estimation of (γ) the radius of cylinder decays which reduces the contact region of cylinder. That is why $f'(\eta)$ enhances. Role of nanoparticle volume fraction (ϕ) on $f'(\eta)$ is displayed in Fig. 3. $f'(\eta)$ is noticed an increasing function of (ϕ). Fig. 4 reports the salient characteristics of mixed convection parameter (λ) in Fig. 4. Here $f'(\eta)$ enhances for larger (λ). Since λ is the combination of buoyancy forces and viscous forces. In fact higher estimation of mixed convection (λ) parameter correspond to decay in viscous forces and so an augmentation in $f'(\eta)$ is distinguished.

Table 1
Thermal characteristics of continuous phase fluid and nanomaterials [2]:

Continuous phase fluid and nanomaterials	Water	Aluminum oxide	Titanium dioxide	Copper
Molecular formula	H_2O	Al_2O_3	Tio_2	Cu
C_P(J/kg K)	4179	765	686.2	385
ρ(kg/m^3)	997.1	3970	4250	8933
k(W/mK)	0.613	40.0	8.954	400.0
$\alpha * 10^7$(m^2/s)	1.47	131.1	30.9	1163.1
$\beta * 10^{-5}$(1/K)	21	0.85	0.9	1.67

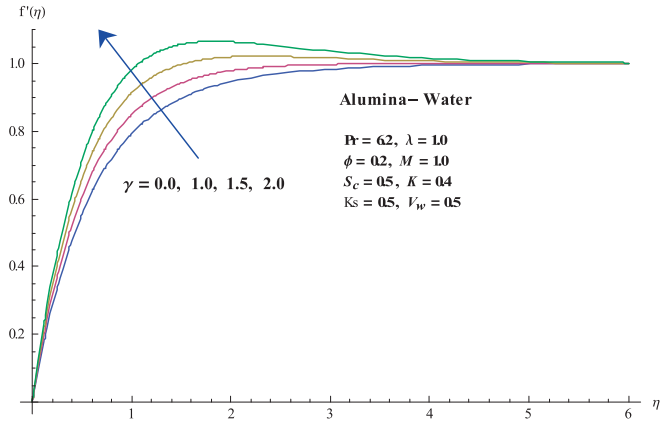

Fig. 2. γ via $f'(\eta)$.

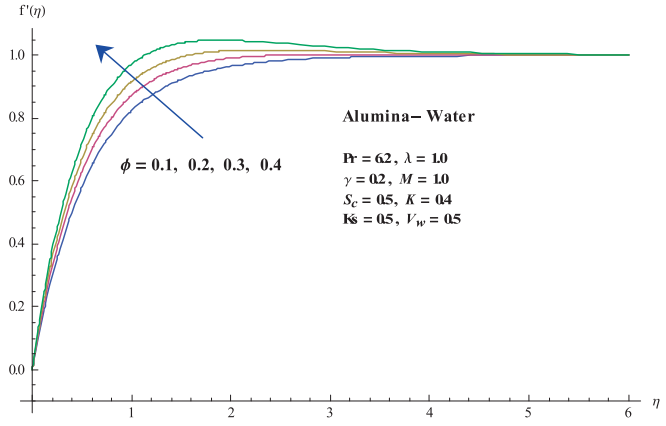

Fig. 3. ϕ via $f'(\eta)$.

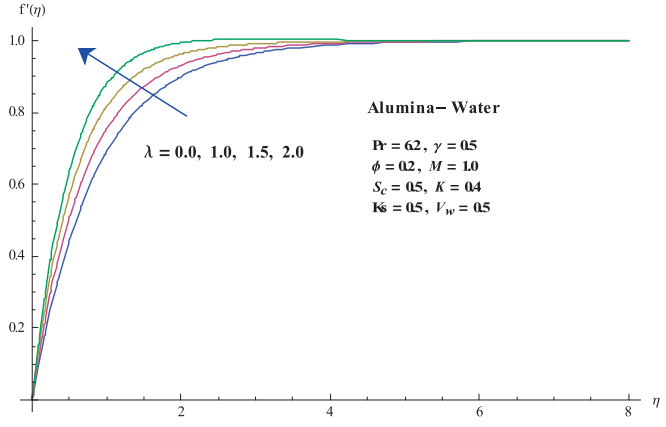

Fig. 4. λ via $f'(\eta)$.

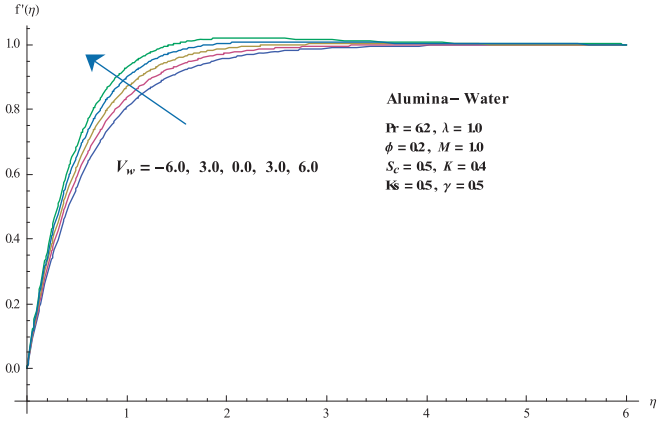

Fig. 5. V_w via $f'(\eta)$.

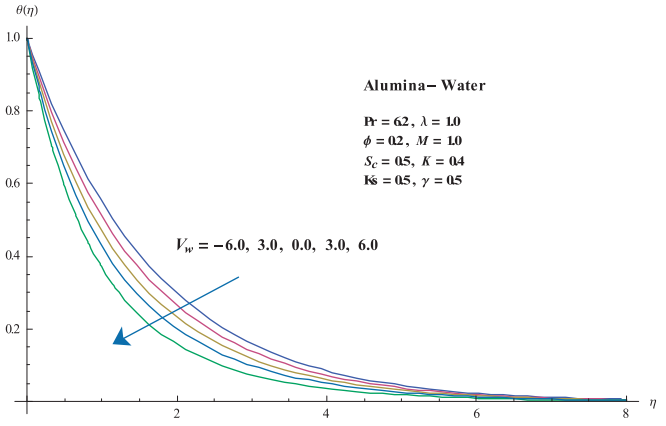

Fig. 6. V_w via $\theta(\eta)$.

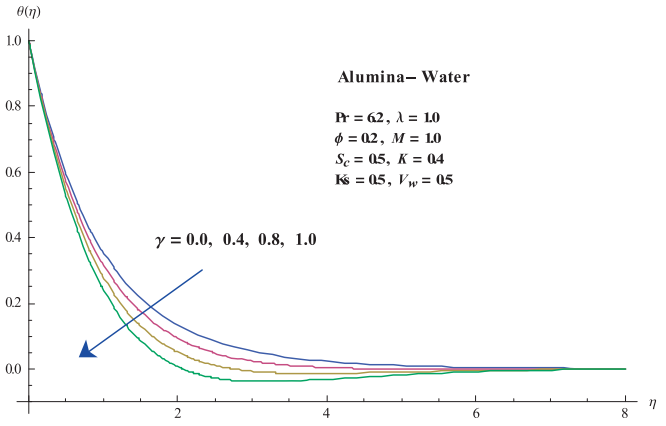

Fig. 7. γ via $\theta(\eta)$.

Characteristics of permeability parameter (V_w) on $f'(\eta)$ is elucidated in Fig. 5. Here velocity distribution enhances for larger (V_w). However opposite trend is observed for temperature $\theta(\eta)$ (see Fig. 6). Effect of curvature parameter (γ) on $\theta(\eta)$ is sketched in Fig. 7. Here $\theta(\eta)$ decreases via (γ). There is a decrease in resistance for larger (γ) and so $\theta(\eta)$ decreases. Fig. 8 demonstrates impact of nanoparticle volume fraction (ϕ) on $\theta(\eta)$. As expected for larger nanoparticle volume fraction (ϕ) there is an increase in thermal conductivity of fluid. As a result both $\theta(\eta)$ and thermal layer thickness are increased. Fig. 9 illustrates decay of temperature and thermal layer thickness for larger mixed convection parameter (λ). Fig. 10 depicts the impact of (M) on $\theta(\eta)$. For larger M there is more resistive type force which slows down the flow. Further $\theta(\eta)$ decreases via M. Fig. 11 presents the behavior of Prandtl number on temperature field. Here temperature is a decreasing function of varying estimation of Prandtl number. Characteristics of curvature (γ) on concentration $g(\eta)$ are displayed in Fig. 12. Here concentration field shows decreasing behavior for rising values of (γ).

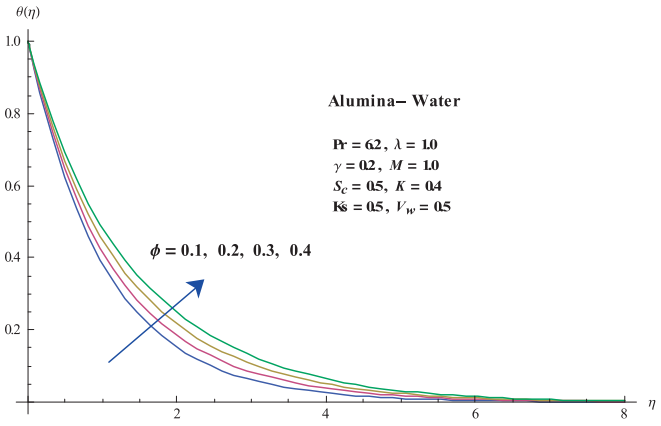

Fig. 8. ϕ via $\theta(\eta)$.

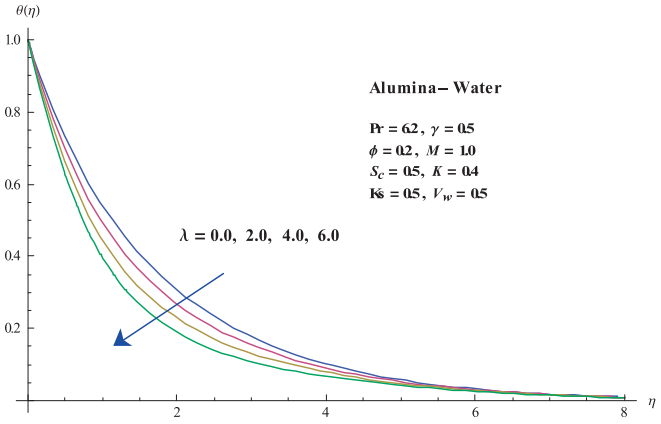

Fig. 9. λ via $\theta(\eta)$.

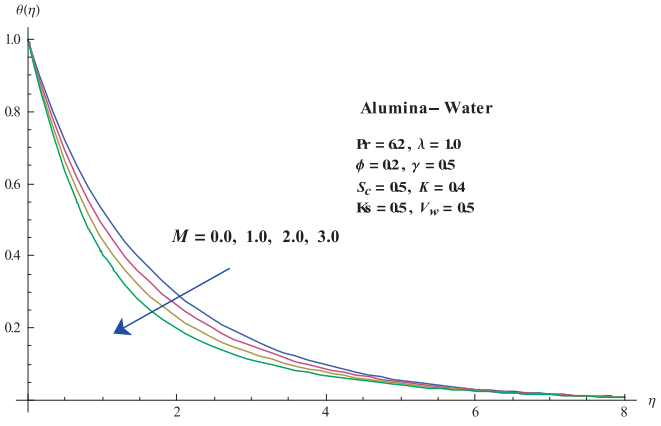

Fig. 10. M via $\theta(\eta)$.

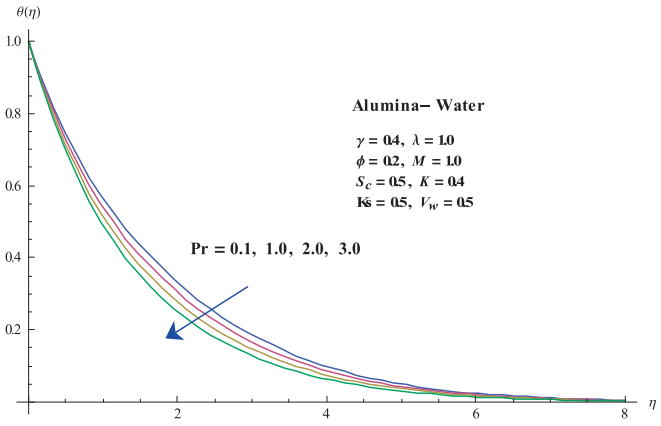

Fig. 11. Pr via $\theta(\eta)$.

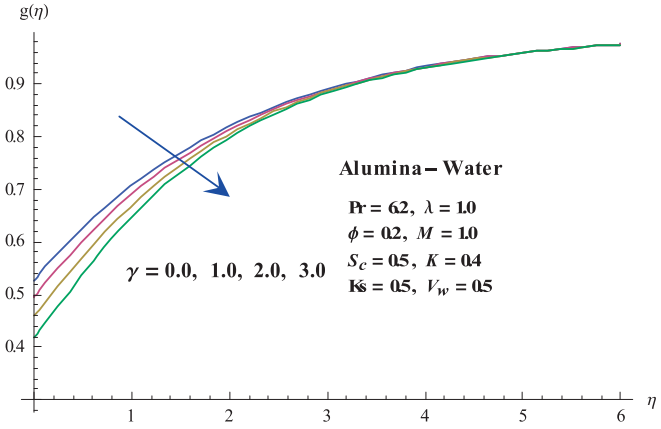

Fig. 12. γ via $g(\eta)$.

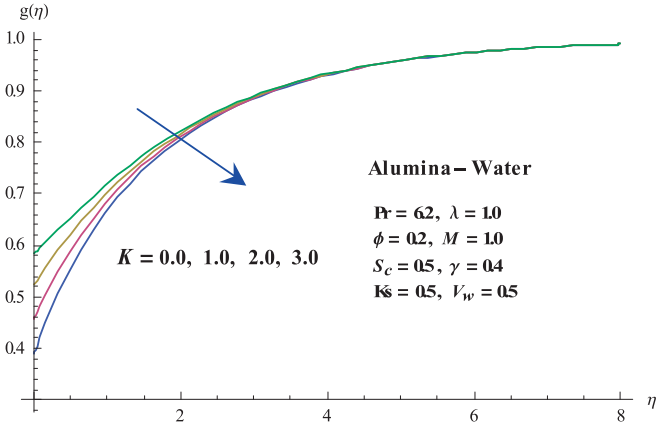

Fig. 13. K via $g(\eta)$.

Influence of homogeneous reaction parameter (K) on $g(\eta)$ is sketched in Fig. 13. Concentration $g(\eta)$ decays while associated layer thickness enhances for larger (K). Behavior of heterogeneous reaction parameter (Ks) on $g(\eta)$ is analyzed in Fig. 14. Here $g(\eta)$ enhances for larger variations of heterogeneous reaction parameter (Ks). Fig. 15 elucidates the variation of (Sc) on $g(\eta)$. As (Sc) is inversely proportional to coefficient of Brownian diffusion. Higher (Sc) corresponds to weaker Brownian diffusion. It give rise to decay in $g(\eta)$. Figs. 16 and 17 correspond to results of (γ) and (M) on surface drag force and heat transfer rtae. It is worth mentioning that both graphs in Figs. 16 and 17 have been plotted for copper-water nanomaterial. It is observed that surface drag force and heat transfer rate are enhanced for larger (γ) and (M).

Conclusions

Following points are the observations of presented study.

- $f'(\eta)$ enhances for higher γ, ϕ and λ.

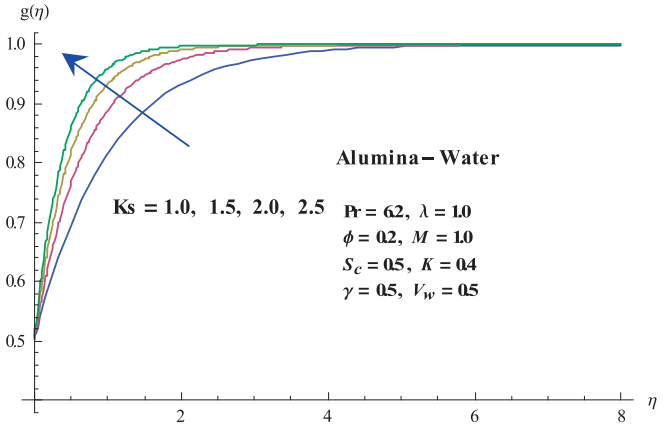

Fig. 14. *Ks* via $g(\eta)$.

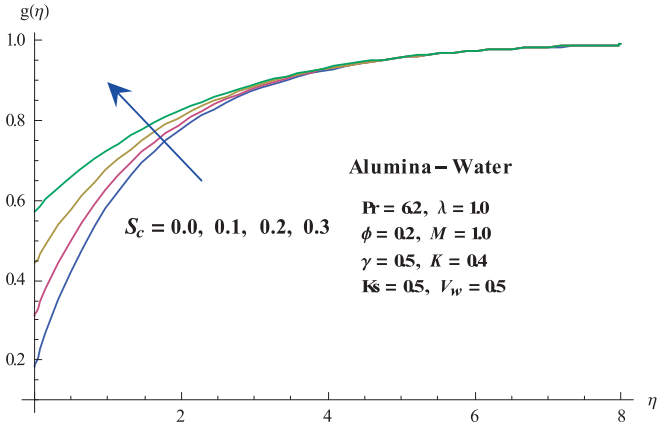

Fig. 15. S_c via $g(\eta)$.

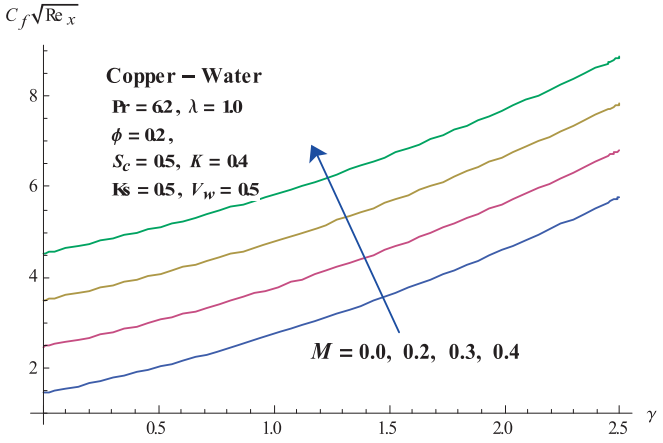

Fig. 16. Effects of γ and M on C_{fx}.

- Larger nanoparticles volume fraction (ϕ) rises $\theta(\eta)$ and thermal layer thickness.
- An increase in curvature (γ) and homogeneous reaction (K) parameters lead to reduce concentration $g(\eta)$.
- Thermal layer thickness is decreased for M and Pr.
- Behavior of $Re_x^{0.5}C_{fx}$ for larger (γ) and (M) is increasing.
- $Re_x^{-0.5}Nu_x$ enhances for larger (γ) and (M).

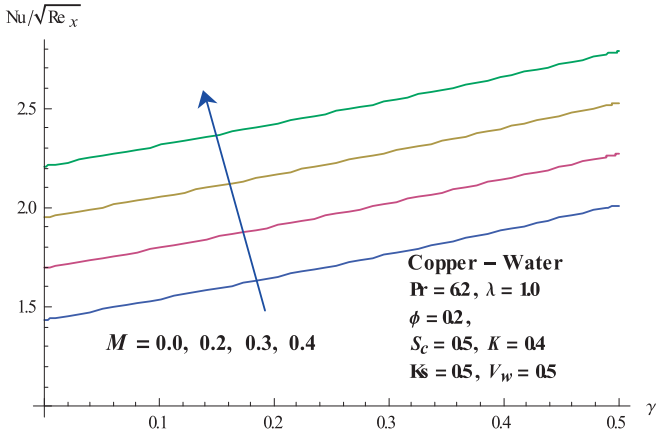

Fig. 17. Effects of γ and M on Nu_x.

References

[1] Choi SUS. Enhancing thermal conductivity of fluids with nanoparticles. ASME Int Mech Eng Congr Exposition 1995;29:99–105.
[2] Buongiorno J. Convective transport in nanofluids. ASME J Heat Transfer 2006;128:240–50.
[3] Kuznetsov AV, Nield DA. Natural convective boundary-layer flow of a nanofluid past a vertical plate. Int J Thermal Sci 2010;49:243–7.
[4] Nield DA, Kuznetsov AV. The Cheng-Minkowycz problem for natural convective boundary layer flow in a porous medium saturated by a nanofluid: a revised model. Int J Heat Mass Transfer 2009;52:5792–5.
[5] Ellahi R, Hassan M, Zeeshan A. Study of natural convection MHD nanofluid by means of single and multi-walled carbon nanotubes suspended in a salt-water solution. IEEE Trans Nanotechnol 2015;14:726–34.
[6] Sheikholeslami M, Hayat T, Alsaedi A. Numerical simulation of nanofluid forced convection heat transfer improvement in existence of magnetic field using lattice Boltzmann method. Int J Heat Mass Transfer 2017;108:1870–83.
[7] Hwang KS, Jang SP, Choi SUS. Flow and convective heat transfer characteristics of water-based Al_2O_3 nanofluids in fully developed laminar flow regime. Int J Heat Mass Transfer 2009;52:193–9.
[8] Kumaresan V, Velraj R, Das SK. Convective heat transfer characteristics of secondary refrigerant based CNT nanofluids in a tubular heat exchanger. Int J Refrig 2012;35:2287–96.
[9] Hatami M, Sheikholeslami M, Ganji DD. Nanofluid flow and heat transfer in an asymmetric porous channel with expanding or contracting wall. J Mol Liq 2014;195:230–9.
[10] Farooq M, Khan MI, Waqas M, Hayat T, Alsaedi A, Khan MI. MHD stagnation point flow of viscoelastic nanofluid with non-linear radiation effects. J Mol Liq 2016;221:1097–103.
[11] Mabood F, Ibrahim SM, Kumar PV, Khan WA. Viscous dissipation effects on unsteady mixed convective stagnation point flow using Tiwari-Das nanofluid model. Results Phys 2017;7:280–7.
[12] Dinarvand S, Pop I. Free-convective flow of copper/water nanofluid about a rotating down-pointing cone using Tiwari-Das nanofluid scheme. Adv Powder Technol 2017;28:900–9.
[13] Hayat T, Khan MI, Alsaedi A, Khan MI. Joule heating and viscous dissipation in flow of nanomaterial by a rotating disk. Int Commun Heat Mass Transfer 2017;89:190–7.
[14] Hayat T, Khan MI, Waqas M, Alsaedi A, Farooq M. Numerical simulation for melting heat transfer and radiation effects in stagnation point flow of carbon–water nanofluid. Comput Methods Appl Mech Eng 2017;315:1011–24.
[15] Khan MI, Hayat T, Khan MI, Alsaedi A. Activation energy impact in nonlinear radiative stagnation point flow of Cross nanofluid. Int Commun Heat Mass Transfer [in press].
[16] Hayat T, Khan MI, Farooq M, Alsaedi A, Yasmeen T. Impact of Marangoni convection in the flow of carbon–water nanofluid with thermal radiation. Int J Heat Mass Transfer 2017;106:810–5.
[17] Waqas M, Khan MI, Hayat T, Alsaedi A. Numerical simulation for magneto Carreau nanofluid model with thermal radiation: a revised model. Comput Methods Appl Mech Eng 2017;324:640–53.
[18] Hayat T, Qayyum S, Khan MI, Alsaedi A. Current progresses about probable error and statistical declaration for radiative two phase flow using Ag-H_2O and Cu-H_2O nanomaterials. Int J Hydrogen Energy 2017;42:29107–20.
[19] Crane LJ. Flow past a stretching plate. Z Angew Math Mech 1970;21:645–7.
[20] Bai Y, Liu X, Zhang Y, Zhang M. Stagnation-point heat and mass transfer of MHD Maxwell nanofluids over a stretching surface in the presence of thermophoresis. J Mol Liq 2016;224:1172–80.
[21] Turkyilmazoglu M. Flow of a micropolar fluid due to a porous stretching sheet and heat transfer. Int J Non-Linear Mech 2016;83:59–64.

[22] Hayat T, Khan MI, Alsaedi A, Khan MI. Homogeneous-heterogeneous reactions and melting heat transfer effects in the MHD flow by a stretching surface with variable thickness. J Mol Liq 2016;223:960–8.
[23] Reddya JVR, Sugunammaa V, Sandeep N, Sulochana C. Influence of chemical reaction, radiation and rotation on MHD nanofluid flow past a permeable flat plate in porous medium. J Niger Math Soc 2016;35:48–65.
[24] Rout BR, Parida SK, Panda S. MHD heat and mass transfer of chemical reaction fluid flow over a moving vertical plate in presence of heat source with convective surface boundary condition. Int J Chem Eng 2013;2013:296834.
[25] Hayat T, Khan MI, Farooq M, Alsaedi A, Waqas M, Yasmeen T. Impact of Cattaneo-Christov heat flux model in flow of variable thermal conductivity fluid over a variable thicked surface. Int J Heat Mass Transfer 2016;99:702–10.
[26] Hayat T, Khan MI, Farooq M, Yasmeen T, Alsaedi A. Stagnation point flow with Cattaneo-Christov heat flux and homogeneous-heterogeneous reactions. J Mol Liq 2016;220:49–55.
[27] Mahanthesh B, Gireesha BJ, Gorla RSR, Abbasi FM, Shehzad SA. Numerical solutions for magnetohydrodynamic flow of nanofluid over a bidirectional non-linear stretching surface with prescribed surface heat flux boundary. J Magn Magn Mater 2016;417:189–96.
[28] Hayat T, Waqas M, Shehzad SA, Alsaedi A. On model of Burgers fluid subject to magneto nanoparticles and convective conditions. J Mol Liq 2016;222:181–7.
[29] Li J, Zheng L, Liu L. MHD viscoelastic flow and heat transfer over a vertical stretching sheet with Cattaneo-Christov heat flux effects. J Mol Liq 2016;221:19–25.
[30] Hayat T, Khan MWA, Alsaedi A, Ayub M, Khan MI. Stretched flow of Oldroyd-B fluid with Cattaneo-Chrsitov heat flux. Results Phys 2017;7:2470–6.
[31] Hayat T, Khan M, Khan MI, Alsaedi A, Ayub A. Electromagneto squeezing rotational flow of Carbon (Cu)-Water (H_2O) kerosene oil nanofluid past a Riga plate: a numerical study. PLoS One 2017;12:e0180976.
[32] Hayat T, Khan MI, Waqas M, Alsaedi A. Mathematical modeling of non-Newtonian fluid with chemical aspects: A new formulation and results by numerical technique. Colloids Surf, A 2017;518:263–72.
[33] Hayat T, Salman S, Khan MI, Alsaedi A. Simulation of ferromagnetic nanomaterial flow of Maxwell fluid. Results Phys 2018;8:34–40.
[34] Hayat T, Salman A, Khan MI, Alsaedi A. Non-Darcy Forchheimer flow of ferromagnetic second grade fluid. Results Phys 2017;7:3419–24.
[35] Khan MI, Hayat T, Alsaedi A. Numerical analysis for Darcy-Forchheimer flow in presence of homogeneous-heterogeneous reactions. Results Phys 2017;7:2644–50.